

## Correlation between electrical activity and the size of rabbit sino-atrial node cells

Haruo Honjo, Mark R. Boyett\* †, Itsuo Kodama ‡ and Junji Toyama

*Departments of Circulation and ‡Humoral Regulation, Research Institute of Environmental Medicine, Nagoya University, Nagoya 464-01, Japan and \*Department of Physiology, University of Leeds, Leeds LS2 9JT, UK*

1. Single cells were isolated from rabbit sino-atrial (SA) node by enzymatic dissociation. Spontaneous action potentials and membrane currents were recorded using the whole-cell patch clamp technique to study the relationship between electrical activity and the size of the cells.
2. The size of SA node cells was estimated by measuring the cell capacitance. The cell capacitance of SA node cells ranged from 21.8 to 61.5 pF with a mean  $\pm$  s.e.m. of  $38.2 \pm 1.3$  pF ( $n = 61$ ).
3. The action potential amplitude, maximum diastolic potential, take-off potential and action potential upstroke velocity were greater in larger cells. The rate of diastolic depolarization was greater and the intrinsic spontaneous activity was faster in larger cells.
4. The density of hyperpolarization-activated current ( $i_f$ ) was greater in larger cells, whereas the density of L-type calcium current was not correlated with the size of SA node cells.
5. TTX-sensitive sodium current ( $i_{Na}$ ) was absent in small cells with a capacitance of less than  $\sim 25$  pF, and the density of  $i_{Na}$  was greater in larger cells.
6. The greater density of  $i_{Na}$  in larger cells may explain the higher upstroke velocity of the action potential in large cells, and the greater density of  $i_f$  and  $i_{Na}$  could be responsible for the faster intrinsic spontaneous activity of large cells. These results suggest that the SA node consists of electrophysiologically heterogeneous pacemaker cells with different electrical membrane properties.

The sino-atrial (SA) node, the physiological pacemaker of the mammalian heart, is an inhomogeneous tissue. Under physiological conditions, the action potential is initiated in the centre of the SA node (the leading pacemaker site) and propagated to the atrial muscle via the periphery of the node. Previous studies with light and electron microscopy (James, 1967; Trantum-Jensen, 1976; Masson-Pévet, Bleeker, Mackaay, Bouman & Houtkooper, 1979; Bleeker, Mackaay, Masson-Pévet, Bouman & Becker, 1980; Masson-Pévet, Bleeker, Besselon, Treysel, Jongasma & Bouman, 1984; Oosthoek, Virágh, Mayen, van Kempen, Lamers & Moorman, 1993) have revealed that SA node cells are morphologically heterogeneous. Typical leading pacemaker cells located in the centre of the SA node are characterized by empty cytoplasm with few organelles and a few poorly organized myofilaments, whereas in the periphery the cells are densely packed with well-organized myofilaments and mitochondria. The cell structure changes gradually from the centre towards the periphery. The size of pacemaker cells is also

different in the centre and the periphery of the SA node: leading pacemaker cells in the centre are small (less than  $8 \mu\text{m}$  in diameter and  $25\text{--}30 \mu\text{m}$  in length) and the cells become larger towards the periphery (Masson-Pévet *et al.* 1979; Bleeker *et al.* 1980; Masson-Pévet *et al.* 1984; Oosthoek *et al.* 1993).

It is well known that spontaneous action potentials recorded from intact SA node preparations of various species are heterogeneous: action potentials from cells in the centre of the node have a smaller amplitude and less negative diastolic potentials associated with a slower upstroke than action potentials from cells in the periphery (Masson-Pévet *et al.* 1979; Bleeker *et al.* 1980; Masson-Pévet *et al.* 1984; Opthof *et al.* 1985; Opthof, de Jonge, Mackaay, Masson-Pévet, Jongasma & Bouman, 1986; Opthof, de Jonge, Jongasma & Bouman, 1987*a*). The configuration of the action potential changes gradually from the leading pacemaker site in the centre towards the periphery. Such a transition of electrical activity from the centre to the periphery could simply

† To whom correspondence should be addressed.

reflect a gradual increase in the electrotonic influence of the surrounding atrial cells (with more hyperpolarized diastolic potentials) from the centre towards the periphery. However, it could also be the result of a regional difference in the electrophysiological properties of SA node tissue. The latter possibility is supported by results from experiments using ligated or dissected small pieces of tissue from different regions of the SA node. In this case, even though the electrotonic influence of the surrounding atrial tissue is removed, there is still a marked difference in the electrophysiological characteristics of tissue from the centre and periphery of the SA node (Kodama & Boyett, 1985; Ophof, van Ginneken, Bouman & Jongasma, 1987*b*). This could be the result of a regional difference in the electrophysiological properties of individual pacemaker cells. However, recent immunohistochemical studies have shown that, in some species, atrial cells are intermingled with SA node pacemaker cells in the peripheral region of the SA node (Oosthoek *et al.* 1993; ten Velde *et al.* 1995). Based on these results, Verheijck (1994) has put forward a new hypothesis: he has suggested that the electrophysiological properties of individual pacemaker cells are uniform throughout the SA node and the apparent regional differences in electrical activity in the intact SA node are the result of a progressive increase in the percentage of intermingling atrial cells towards the periphery giving rise to a progressive increase in their hyperpolarizing influence from the centre towards the periphery of the node.

We have investigated the mechanisms underlying the electrophysiological heterogeneity in the intact SA node by studying the relationship between electrical activity and the size of isolated rabbit SA node cells. Contrary to Verheijck's (1994) hypothesis, the results obtained suggest that the SA node consists of electrophysiologically heterogeneous pacemaker cells with different membrane properties. Preliminary results of this work have been published in abstract form (Honjo & Boyett, 1992; Honjo, Boyett & Kodama, 1996).

## METHODS

### Cell isolation

Single SA node cells were enzymatically isolated from adult rabbit hearts by methods similar to those described previously (Honjo, Kodama, Zang & Boyett, 1992; Watanabe, Honjo, Anno, Boyett, Kodama & Toyama, 1995). In brief, a New Zealand White rabbit (6–10 weeks old) of either sex, weighing 1.0–1.5 kg, was anaesthetized with an intravenous injection of sodium pentobarbitone (40 mg kg<sup>-1</sup>). Heparin (300–1000 u kg<sup>-1</sup>) was injected at the same time. After the rabbit was exsanguinated, the heart was dissected out and placed in oxygenated Tyrode solution at 36 °C. The SA node region was then isolated and cut into several strips perpendicular to the crista terminalis. From each strip the epicardial surface including atrial muscle was carefully removed under a dissecting microscope. The SA node tissue strips were immersed in nominally Ca<sup>2+</sup>-free Tyrode solution until spontaneous beating ceased, and then transferred to an enzyme solution containing collagenase and elastase. In some cases, protease was added to the enzyme solution. The preparations were digested with enzymes for 40 min at 36 °C. The digested strips were placed in a

small amount of high K<sup>+</sup>, low Cl<sup>-</sup> Kraft-Brihue (KB) solution and teased to produce a cell suspension. The cells were kept at 4 °C before they were used experimentally.

### Electrophysiological measurements

Membrane potential and currents were recorded using the whole-cell patch clamp technique. An Axopatch-1C amplifier (Axon Instruments) was used. The resistance of the patch pipettes ranged from 2 to 4 M $\Omega$  when filled with the internal solution. The pipette and cell capacitance and the series resistance (> 60%) were electronically compensated. The current signal was filtered by a Bessel-type low-pass filter with a cut-off frequency of 10 kHz (-3 dB). The seal resistance was routinely measured at the beginning of each experiment and ranged from ~15 to ~20 G $\Omega$ . When the seal resistance was less than 10 G $\Omega$  or 10 times the value of the input resistance, the data were discarded. Membrane potential and current were recorded using a personal computer (via a CED 1401; Cambridge Electronic Design, Cambridge, UK) running Signal Averager software (Cambridge Electronic Design) at various sampling rates (2–50 kHz) and stored on videotape (via a Neurocorder DR-886; Neuro Data Instruments, New York, NY, USA) for later analysis. Spontaneous action potentials were recorded at 35  $\pm$  0.2 °C and various measurements were made including the action potential amplitude, action potential overshoot, maximum diastolic potential (MDP), action potential duration at the half-repolarization level and spontaneous cycle length (the time interval between successive spontaneous action potentials). The rate of diastolic depolarization was calculated during the first two-thirds of the diastolic interval during which the slope of the pacemaker potential is roughly constant. The take-off potential, the membrane potential at which a spontaneous action potential is initiated, was estimated from the intersection of two straight lines fitted to the diastolic depolarization and to the upstroke of the action potential (see the inset of Fig. 4*B*). The first derivative of membrane potential was calculated from digitized membrane potential data (sampling frequency was 2–5 kHz) and its peak value was taken as the maximum upstroke velocity. Mean values of these action potential characteristics were calculated from at least five successive action potentials. Cell capacitance ( $C_m$ ), which is proportional to the cell surface area, was calculated by fitting a single exponential function to the decay phase of the transient capacity current in response to  $\pm 5$  or  $\pm 10$  mV voltage clamp pulses from a holding potential of -40 mV. In experiments to record hyperpolarization-activated current ( $i_t$ ) and L-type Ca<sup>2+</sup> current ( $i_{Ca}$ ), either hyperpolarizing or depolarizing voltage clamp pulses (300 ms in duration) to various potentials were applied from a holding potential of -40 mV. The amplitude of  $i_t$  was defined as the increase in inward current during hyperpolarizing pulses, and  $i_{Ca}$  was measured simply as the peak of the inward current during depolarizing pulses. These experiments were carried out at 35  $\pm$  0.2 °C. Tetrodotoxin (TTX)-sensitive Na<sup>+</sup> current ( $i_{Na}$ ) was elicited by 30 ms depolarizing voltage clamp pulses from a holding potential of -60 mV at room temperature (22–26 °C; see Results). Measurements of  $i_{Ca}$ ,  $i_t$  and  $i_{Na}$  were made under physiological ionic conditions; cells were superfused with normal Tyrode solution and the same K<sup>+</sup>-rich pipette solution used to record action potentials was employed. In order to minimize interference from rundown of membrane currents, only action potentials and membrane currents recorded within 3 min of the rupture of the patch were analysed unless specified otherwise.

### Solutions and drugs

Normal Tyrode solution contained (mM): 136.9 NaCl, 5.4 KCl, 1.8 CaCl<sub>2</sub>, 0.5 MgCl<sub>2</sub>, 0.33 NaH<sub>2</sub>PO<sub>4</sub>, 5 Hepes and 10 glucose (pH 7.4). Ca<sup>2+</sup>-free Tyrode solution was made by omitting CaCl<sub>2</sub>

from the normal Tyrode solution. Enzyme solution consisted of  $\text{Ca}^{2+}$ -free Tyrode solution plus collagenase (250–400 U  $\text{ml}^{-1}$ ; Yakult, Tokyo, Japan) and elastase (12–35 U  $\text{ml}^{-1}$ , Sigma, Type IIA) and in some cases protease (0.8–1.0 U  $\text{ml}^{-1}$ , Sigma Type XIV). KB solution contained (mM): 20 taurine, 70 L-glutamic acid, 25 KCl, 10  $\text{KH}_2\text{PO}_4$ , 3  $\text{MgCl}_2$ , 0.5 EGTA, 10 Hepes and 10 glucose (pH 7.4). The pipette solution contained (mM): 140 KCl, 3 MgATP, 0.4  $\text{Na}_2\text{GTP}$ , 11 Hepes, 1  $\text{CaCl}_2$  and 11 EGTA (pCa 8, pH 7.2). The liquid junction potential between normal Tyrode solution and the pipette solution was measured experimentally (–4 mV) and was corrected. TTX was purchased from Sankyo (Tokyo, Japan).

### Statistics

Data are presented as means  $\pm$  s.e.m. (number of cells) unless otherwise indicated. Statistical analysis was performed by a linear regression analysis and values of  $P < 0.05$  were considered to indicate significance. The fitting of a normal distribution to the histogram of cell capacitance in Fig. 1 was tested by a  $\chi^2$  analysis.

## RESULTS

Enzymatic digestion of rabbit SA node tissue yielded morphologically different types of cells such as spindle-, spider- or rod-shaped cells as demonstrated by other investigators (Irisawa, Brown & Giles, 1993), and some of these cells (~5–15%) showed regular and stable spontaneous beating when superfused with normal Tyrode solution. Only cells showing regular and spontaneous beating were used; they were spindle-shaped, with no obvious or faint striations, 40–120  $\mu\text{m}$  in length and 4–9  $\mu\text{m}$  in width and typically had a small central bulge. Denyer (1989) has demonstrated that these are single cells because they have a single nucleus in the central bulge. Cells with many long, thin extrusions (spider cells) were neglected, since they might be undigested paired cells or clusters of cells (Denyer, 1989; Denyer & Brown, 1990). Clearly striated rod-shaped cells with a length of more than ~150  $\mu\text{m}$ , which are similar to those isolated from the crista terminalis (Giles & van Ginneken, 1985), were also rejected. The capacitance of the cells ranged from 21.8 to 61.5 pF

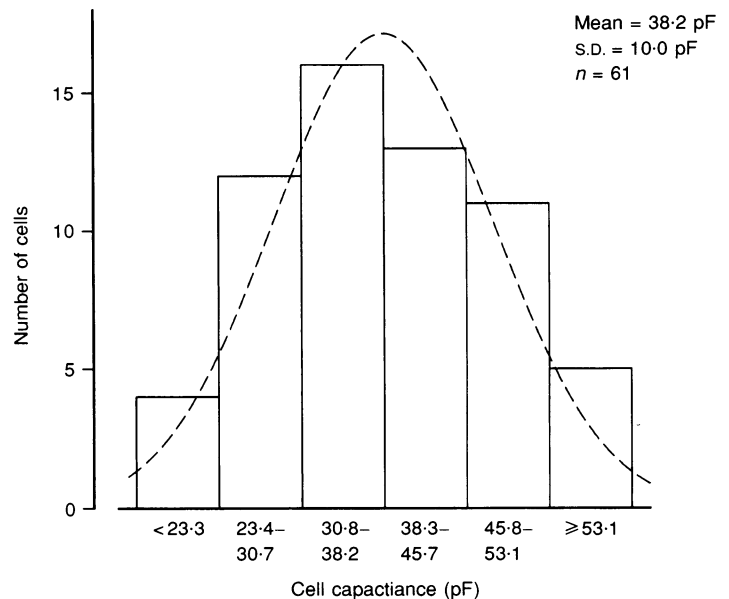
with a mean  $\pm$  s.d. of  $38.2 \pm 10.0$  pF ( $n = 61$ ). The distribution of cell capacitance was well fitted by a normal distribution curve (Fig. 1,  $P < 0.05$ ), suggesting that these cells belong to a single population. The cells showed slowly activating inward current ( $i_f$ ) during hyperpolarizing voltage clamp pulses (see Fig. 6) and a high input resistance ranging from 1.5 to 3.5 G $\Omega$  at –40 mV reflecting a lack of the inwardly rectifying  $\text{K}^+$  current  $i_{\text{K},1}$ . This combination of morphological and electrophysiological characteristics indicates that the cells were SA node pacemaker cells (Irisawa *et al.* 1993).

### Correlation between action potential characteristics and cell size

Representative examples of spontaneous action potentials recorded from different SA node cells of a rabbit are shown in Fig. 2 – membrane potential is shown in the top trace and the first derivative of the membrane potential in the bottom trace. Data in the left-hand panel of Fig. 1 were obtained from a small cell whose capacitance was 22.0 pF. The action potential amplitude, maximum diastolic potential (MDP) and maximum upstroke velocity of this cell were 76.0 mV, –50.6 mV and 6.4  $\text{V s}^{-1}$ , respectively. These values are comparable to those recorded from the centre of the intact SA node and it is known that, in the centre, the cells are small (Masson-Pévet *et al.* 1979; Bleeker *et al.* 1980; Masson-Pévet *et al.* 1984; Oosthoek *et al.* 1993). The spontaneous cycle length of this cell was 377 ms. This is consistent with the possibility that the cell was derived from the centre of the node (see Discussion). Action potentials recorded from a relatively large cell having a capacitance of 57.5 pF are shown in the right-hand panel of Fig. 2. This cell had a larger action potential amplitude (95.5 mV), a more negative MDP (–61.9 mV) and a larger maximum upstroke velocity (33.9  $\text{V s}^{-1}$ ) than those of the small cell shown in the left-hand panel. These values are comparable to those recorded from the periphery of the intact SA node and it is known that in the periphery the cells are larger

**Figure 1**

Histogram of the cell capacitance of the 61 SA node cells isolated from 22 rabbits used in the present study. The dashed line shows the best-fit normal distribution curve.



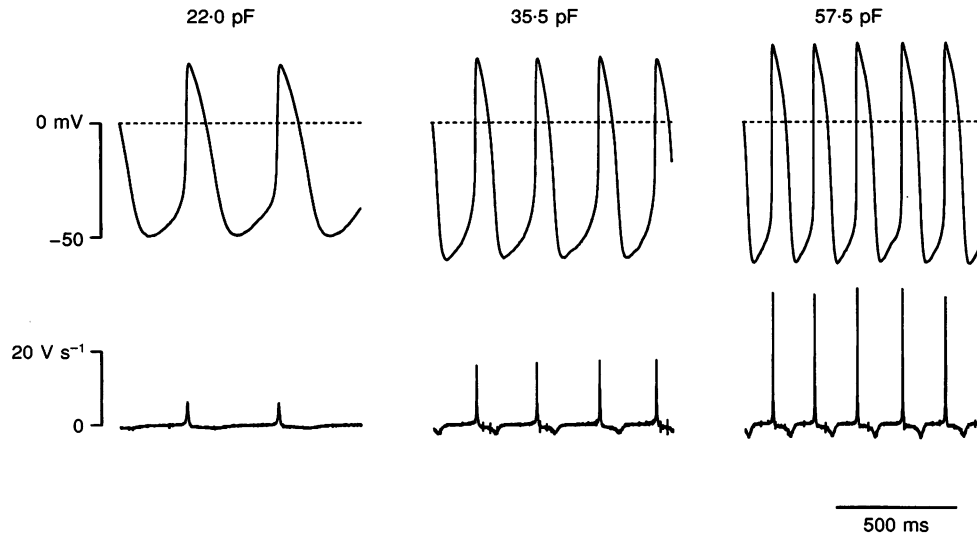


**Figure 2.** Spontaneous action potentials recorded from three SA node cells of different size

Top, membrane potential. Bottom, first derivative of the membrane potential. The cell capacitance is shown above each record.

than those in the centre (Masson-Pévet *et al.* 1979; Bleeker *et al.* 1980; Masson-Pévet *et al.* 1984; Oosthoek *et al.* 1993). The spontaneous cycle length of this large cell was much shorter (173 ms) than that of the small cell (377 ms). This is consistent with the possibility that the cell was derived from

the periphery of the node (see Discussion). Action potentials recorded from an intermediate size cell ( $C_m$ , 35.5 pF) are shown in the middle panel of Fig. 2 – the action potential characteristics (action potential amplitude, MDP, maximum upstroke velocity and spontaneous cycle length) lie between

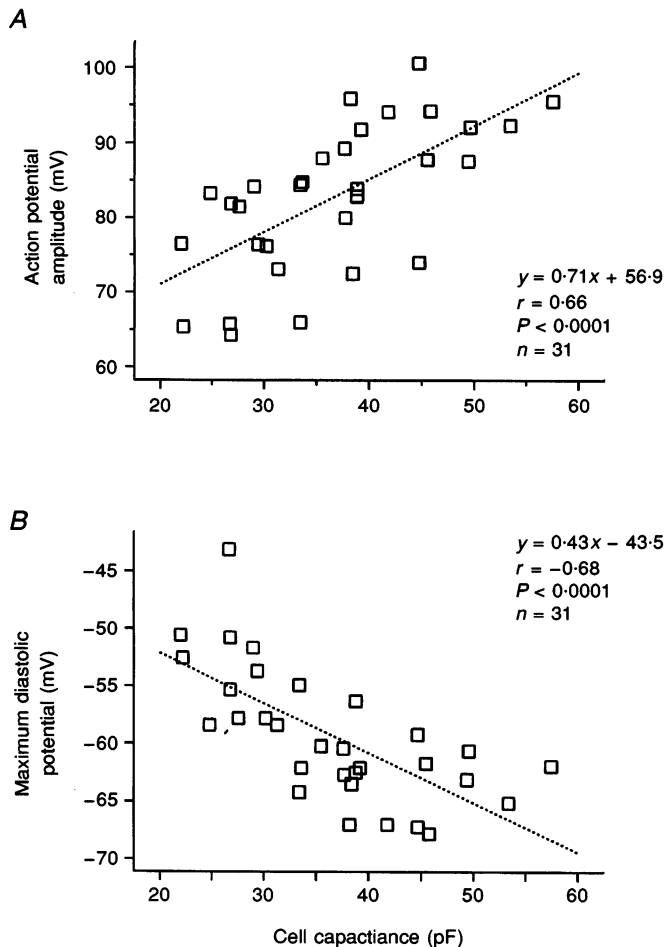


**Figure 3.** Correlation between action potential amplitude and cell size

Plots of the amplitude of the action potential (*A*) and the MDP (*B*) against the cell capacitance in 31 SA node cells. The dotted lines were fitted by linear regression. In this and other figures the results of a linear regression are shown as an inset.

those of the smaller and larger cells. This suggests that the action potential configuration of SA node pacemaker cells varies depending on cell size.

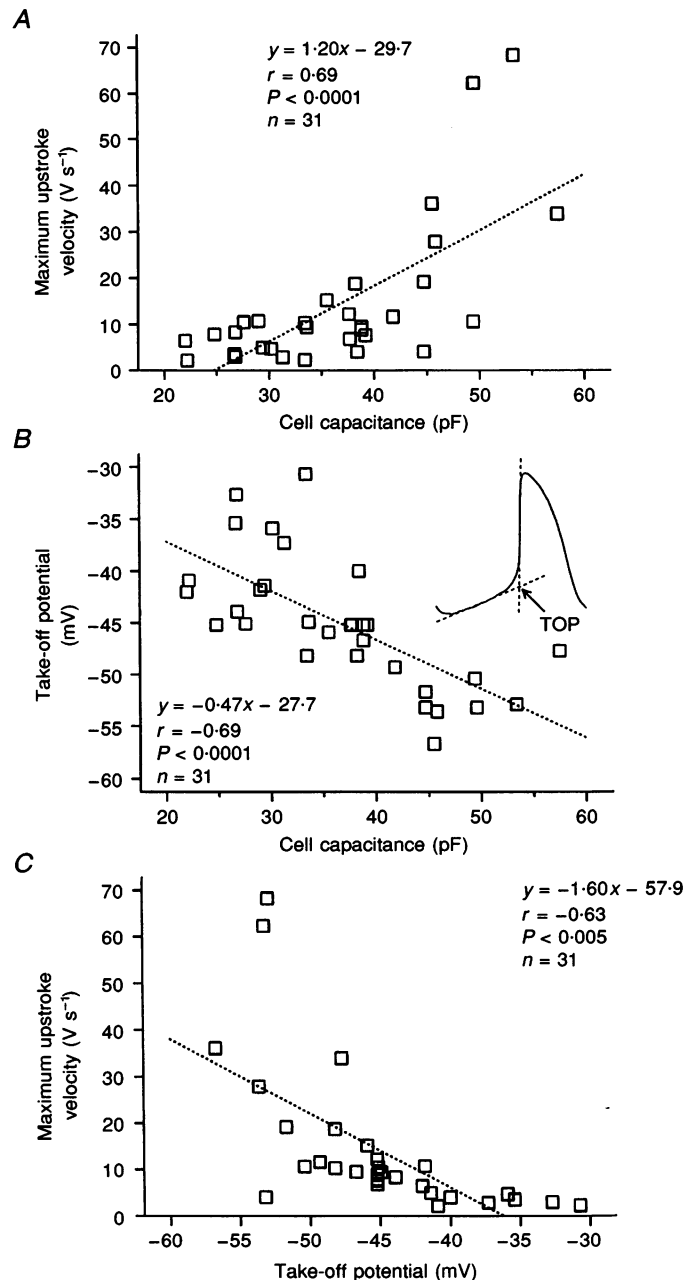
The relationship between action potential characteristics and cell capacitance was investigated in thirty-one SA node cells from seventeen rabbits ( $C_m$ , 22.2–57.5 pF; mean  $\pm$  s.e.m.,  $36.6 \pm 1.7$  pF) – the results are summarized in Figs 3–5. Figure 3 shows the relationship between the size of action potentials and cell capacitance. Action potential amplitude was significantly correlated with cell capacitance ( $r = 0.66$ ,  $P < 0.0001$ ,  $n = 31$ ); the action potential amplitude was greater in larger SA node cells (Fig. 3A). The overshoot of the action potential ranged from +10.8 to +33.4 mV (mean  $\pm$  s.e.m.,  $+23.5 \pm 1.3$  mV). There was no significant correlation between the overshoot and cell capacitance ( $r = 0.34$ ,  $P > 0.05$ ,  $n = 31$ ). This suggests that the change

in action potential amplitude with cell size could be due to a variation of the MDP. As expected, the MDP of SA node cells was significantly correlated with cell capacitance ( $r = -0.68$ ,  $P < 0.0001$ ,  $n = 31$ ); the MDP was more negative in larger cells (Fig. 3B).

Figure 4 shows relationships between measurements concerned with the upstroke phase of the action potential and cell capacitance. The maximum upstroke velocity obtained from different SA node cells varied over a wide range from 2.1 to 68.3  $V s^{-1}$ , and was significantly correlated with cell capacitance ( $r = 0.69$ ,  $P < 0.0001$ ,  $n = 31$ ; Fig. 4A); relatively small SA node cells with a capacitance of less than 30 pF had a maximum upstroke velocity of 10  $V s^{-1}$  or less, and some larger cells had a much greater maximum upstroke velocity (of more than 60  $V s^{-1}$ ). It is possible that the upstroke of cells with a low upstroke

**Figure 4. Correlation between measurements concerned with the upstroke phase of the action potential and cell size**

A and B, plots of the maximum upstroke velocity (A) and the take-off potential (B) against the cell capacitance in 31 SA node cells. The take-off potential (TOP) was calculated from the intersection of a line fitted to the diastolic depolarization and a line fitted to the action potential upstroke, as shown in the inset. C, plot of the maximum upstroke velocity against the take-off potential. The dotted lines were fitted by linear regression.



velocity was generated by  $i_{Ca}$ , whereas the upstroke of cells with a high upstroke velocity was generated by  $i_{Na}$ . Since  $i_{Ca}$  and  $i_{Na}$  are known to have different thresholds, we examined the relationship between the take-off potential and cell capacitance. As shown in Fig. 4B, the take-off potential was significantly correlated with cell capacitance ( $r = -0.69$ ,  $P < 0.0001$ ,  $n = 31$ ); the take-off potential was more negative in larger SA node cells. As expected from these correlations between the maximum upstroke velocity or the take-off potential and cell capacitance, the maximum upstroke velocity was significantly correlated with the take-off potential ( $r = -0.63$ ,  $P < 0.005$ ,  $n = 31$ , Fig. 4C): the maximum upstroke velocity of cells with a take-off potential less negative than  $\sim -45$  mV was less than  $10 \text{ V s}^{-1}$  – this is consistent with  $i_{Ca}$  being responsible for the upstroke of the action potential. The maximum upstroke

velocity of cells having a take-off potential more negative than  $\sim -55$  mV could be greater than  $60 \text{ V s}^{-1}$  – this is consistent with  $i_{Na}$  being responsible for the upstroke phase of the action potential.

The action potentials shown in Fig. 2 suggest that the spontaneous cycle length is shorter in larger cells. Figure 5A demonstrates that the spontaneous cycle length was significantly correlated with cell capacitance in thirty-one SA node cells ( $r = -0.71$ ,  $P < 0.00001$ ,  $n = 31$ ); the spontaneous cycle length was shorter in larger cells. This suggests that the spontaneous rate is paradoxically faster in larger cells (possibly from the periphery of the node) than in smaller cells (possibly from the leading pacemaker site, the centre, of the intact SA node – see Discussion). Since the spontaneous cycle length of SA node cells is theoretically determined by the action potential duration, the slope of the

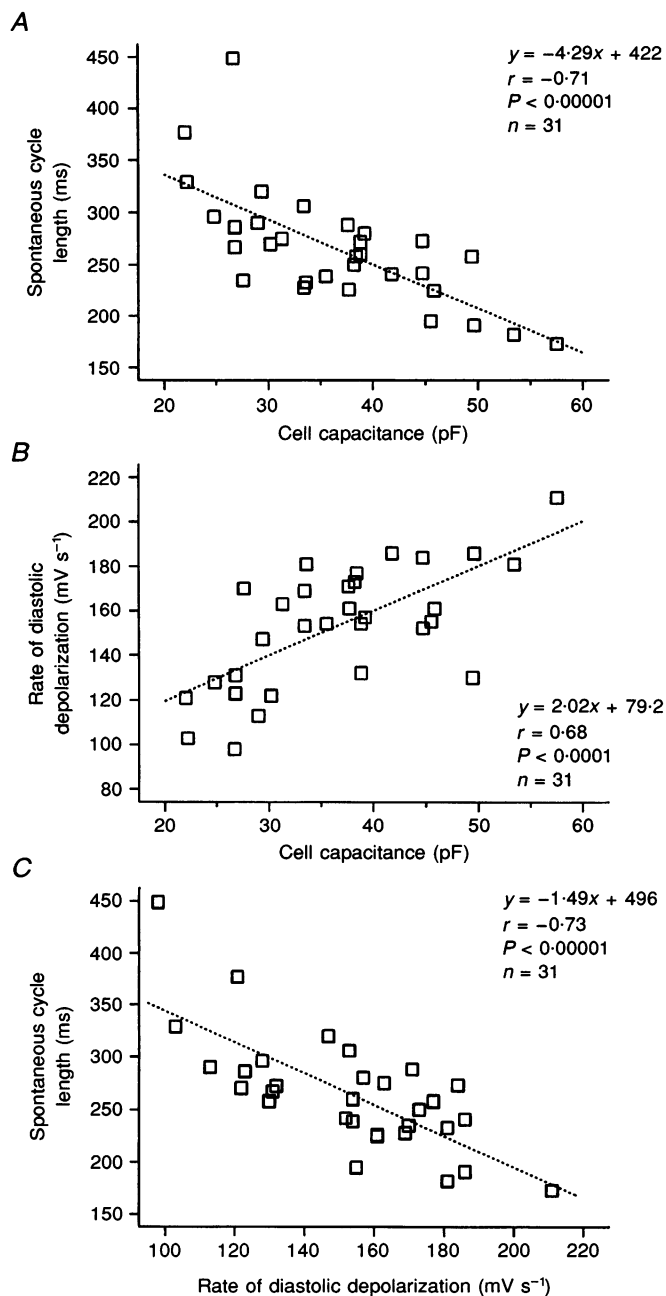


**Figure 5. Correlation between the rate of the spontaneous activity and cell size**

A and B, plots of the spontaneous cycle length (A) and the rate of diastolic depolarization (B) against the cell capacitance in 31 SA node cells. C, plot of the spontaneous cycle length against the rate of diastolic depolarization. The dotted lines were fitted by linear regression.

pacemaker potential (the rate of diastolic depolarization) and the difference in membrane potential between the MDP and take-off potential, relationships between these three measurements and cell capacitance were investigated. There was no significant correlation between action potential duration and cell capacitance ( $r = -0.08$ ,  $P > 0.5$ ,  $n = 31$ ) or the difference in membrane potential between the MDP and the take-off potential and cell capacitance ( $r = -0.35$ ,  $P > 0.05$ ,  $n = 31$ ). On the other hand, the rate of diastolic depolarization was significantly correlated with cell capacitance ( $r = 0.68$ ,  $P < 0.0001$ ,  $n = 31$ ); the rate of diastolic depolarization was greater in larger SA node cells (Fig. 5B). This suggests that the spontaneous cycle length of SA node cells is determined by the rate of diastolic depolarization. This is confirmed by the highly significant correlation between spontaneous cycle length and the rate of diastolic depolarization as shown in Fig. 5C ( $r = -0.73$ ,  $P < 0.00001$ ,  $n = 31$ ).

In order to understand the ionic mechanisms underlying these cell size-dependent variations in the electrical activity of isolated SA node cells, relationships between the density

of various membrane currents involved in the generation of the spontaneous action potential and cell size were investigated.

### Correlation between $i_f$ density and cell size

First, we examined the relationship between the density of  $i_f$  and the size of isolated SA node cells. Figure 6A shows two sets of superimposed current traces in response to hyperpolarizing voltage clamp pulses (300 ms in duration) obtained from small and large SA node cells with capacitances of 22.4 and 44.7 pF, respectively. The two cells were obtained from the same rabbit. The amplitude of  $i_f$  was defined as the increase in inward current from the beginning to the end of the 300 ms pulses. The current-voltage relationships of  $i_f$  obtained from these two SA node cells are shown in the bottom panel of Fig. 6A (current density - current amplitude normalized by  $C_m$  - is plotted against the membrane potential of the 300 ms pulse). The density of  $i_f$  at each potential level was greater in the larger cell. On the other hand, the threshold potential for the activation of  $i_f$  was approximately the same in the two cases. Figure 6B shows the relationship between the

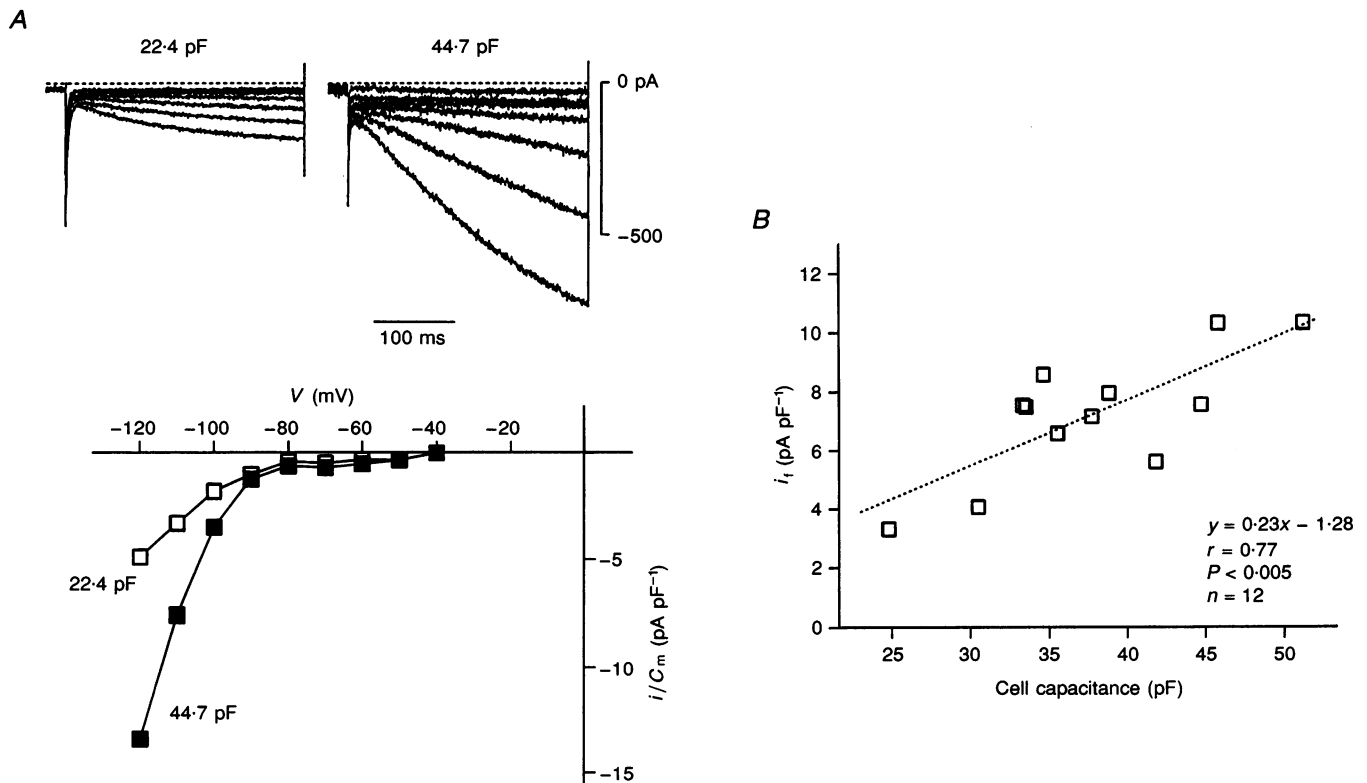


**Figure 6.** Correlation between the density of  $i_f$  and cell size

A, comparison of  $i_f$  recorded from small ( $C_m$ , 22.4 pF) and large ( $C_m$ , 44.7 pF) SA node cells. Top panels, superimposed current traces in response to hyperpolarizing voltage clamp pulses to various potentials (ranging from  $-50$  to  $-120$  mV in 10 mV increments) from a holding potential of  $-40$  mV. The cell capacitance is shown above the records. Bottom panel, current-voltage relationships for  $i_f$  in the two cells. The density of  $i_f$  (current amplitude normalized by  $C_m$ ) is plotted. B, relationship between the density of  $i_f$  measured at  $-110$  mV and cell capacitance in 12 SA node cells. The dotted line was fitted by linear regression.

density of  $i_f$  and cell size in twelve SA node cells from three rabbits. In this graph, the density of  $i_f$  measured at  $-110$  mV is plotted against the cell capacitance ( $C_m$ ,  $24.8$ – $51.2$  pF; mean  $\pm$  s.e.m.,  $37.7 \pm 2.1$  pF,  $n = 12$ ). The density of  $i_f$  was significantly correlated with cell capacitance ( $r = 0.77$ ,  $P < 0.005$ ,  $n = 12$ ); the density of  $i_f$  was greater in larger SA node cells.

#### Correlation between $i_{Ca}$ density and cell size

The relationship between the density of  $i_{Ca}$  and cell size was investigated in the same set of SA node cells as used to record  $i_f$ . In experiments to record  $i_{Ca}$ , depolarizing voltage clamp pulses (300 ms in duration) were applied from a holding potential of  $-40$  mV. The amplitude of  $i_{Ca}$  was measured as the peak inward current during the depolarizing pulses. To test for cell size-dependent differences in  $i_{Ca}$ , twelve cells from three rabbits were divided into two groups: small cells with a capacitance of less than  $35.0$  pF (mean  $\pm$  s.e.m.,  $31.3 \pm 1.8$  pF,  $n = 5$ ) and large cells with a capacitance of more than  $35.0$  pF (mean  $\pm$  s.e.m.,  $42.2 \pm 2.1$  pF,  $n = 7$ ). The amplitude of  $i_{Ca}$  was compared in the two groups. Figure 7A shows the

current–voltage relationship of  $i_{Ca}$  in the two groups of cells. The absolute amplitude of  $i_{Ca}$  is plotted in the top panel and the density of  $i_{Ca}$  (current amplitude normalized by  $C_m$ ) is shown in the bottom panel. Although the absolute amplitude of  $i_{Ca}$  was less in the smaller cells, the density of  $i_{Ca}$  was similar in the two groups at the various potentials. Figure 7B summarizes the individual results obtained from the twelve SA node cells; the density of  $i_{Ca}$  measured at  $0$  mV is plotted against the cell capacitance. There was no significant correlation between the density of  $i_{Ca}$  and cell capacitance ( $r = -0.14$ ,  $P > 0.5$ ,  $n = 12$ ). Similar results were obtained if  $i_{Ca}$  was measured as the difference between the peak inward current and the current at the end of the 300 ms depolarizing pulses. In this series of experiments there was also no significant correlation between cell capacitance and either the holding current at  $-40$  mV or the current at the end of the  $0$  mV pulse.

#### Correlation between $i_{Na}$ density and cell size

As shown earlier, the maximum upstroke velocity of large cells can exceed  $60$  V s $^{-1}$  and it is possible that  $i_{Na}$  is responsible for the upstroke in these cells. In small cells,

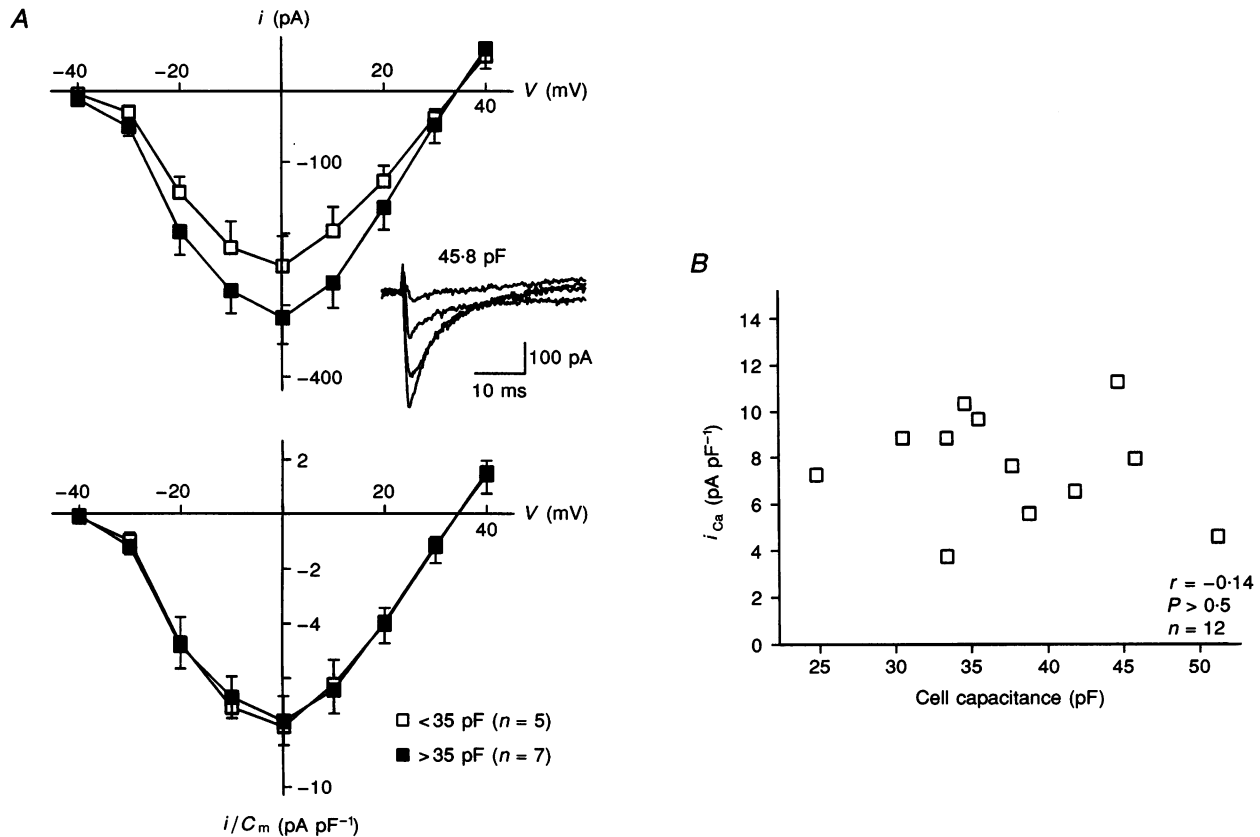


**Figure 7.** Relationship between the density of  $i_{Ca}$  and cell size

A, current–voltage relationships for  $i_{Ca}$  obtained from a group of small cells with a capacitance of less than  $35$  pF ( $n = 5$ ) and a group of large cells with a capacitance of more than  $35$  pF ( $n = 7$ ). Means  $\pm$  s.e.m. are shown of the amplitude of  $i_{Ca}$  (top panel) and the density of  $i_{Ca}$  (current amplitude normalized by  $C_m$ , bottom panel). The inset shows superimposed records of membrane currents (predominantly  $i_{Ca}$ ) in response to depolarizing voltage clamp pulses to  $+40$ ,  $+20$ ,  $0$  and  $-20$  mV from a holding potential of  $-40$  mV obtained from an SA node cell with a capacitance of  $45.8$  pF. B, relationship between the density of  $i_{Ca}$  measured at  $0$  mV and cell capacitance in 12 SA node cells.

however, the maximum upstroke velocity is less than  $10 \text{ V s}^{-1}$  – in these cases the low upstroke velocity can be explained by the absence of  $i_{\text{Na}}$  as a result of either the voltage-dependent inactivation of  $i_{\text{Na}}$  due to the less negative diastolic potentials of small cells or the absence of  $\text{Na}^+$  channels in these cells. To distinguish between these possibilities, we investigated the relationship between the density of  $i_{\text{Na}}$  and the size of SA node cells. To improve voltage control during measurement of  $i_{\text{Na}}$ ,  $i_{\text{Na}}$  was recorded from a holding potential of  $-60 \text{ mV}$ , at which there is partial inactivation of  $i_{\text{Na}}$ , and at a low temperature ( $22\text{--}26^\circ\text{C}$  rather than  $35^\circ\text{C}$  as used in the remainder of the study). The extracellular and intracellular solutions were the same as those used in the remainder of the study.

Figure 8 shows recordings of TTX-sensitive  $i_{\text{Na}}$  present in a relatively large SA node cell ( $C_m$ ,  $54.6 \text{ pF}$ ). Superimposed records of membrane currents before and after the

application of  $20 \mu\text{M}$  TTX are shown in Fig. 8A. Under control conditions, depolarizing voltage clamp pulses activated a large inward current which rapidly activated and inactivated. TTX at  $20 \mu\text{M}$  completely abolished the fast inward current, which indicates that this current is the TTX-sensitive  $i_{\text{Na}}$ . The TTX-sensitive component of the current was obtained by subtraction and is shown in Fig. 8B: the difference currents are shown in the upper panel and the current–voltage relationship of the peak inward difference current is shown in the lower panel. After the block of  $i_{\text{Na}}$  by  $20 \mu\text{M}$  TTX, at very positive potentials, there remained outward current with slow inactivation (possibly the transient outward current; Denyer & Brown, 1990; Ito & Ono, 1995) and, at less positive potentials, inward current (presumably  $i_{\text{Ca}}$ ). The inward current (at slow and fast time bases) is shown in the two lower panels of Fig. 8A.

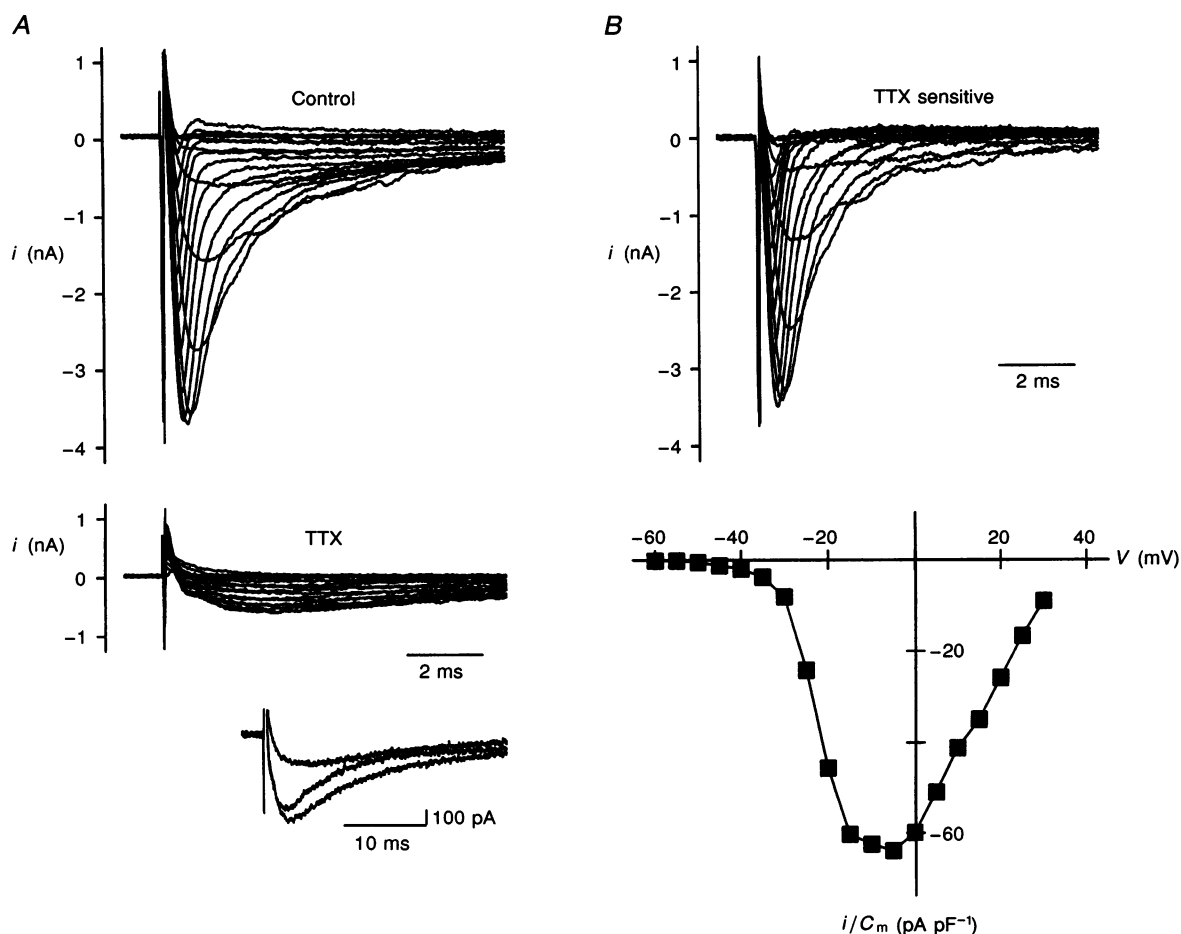


**Figure 8.** TTX-sensitive  $i_{\text{Na}}$  in an SA node cell with a capacitance of  $54.6 \text{ pF}$

A, superimposed records of membrane current in response to depolarizing voltage clamp pulses to various potentials (ranging from  $-55$  to  $+30 \text{ mV}$  in  $5 \text{ mV}$  increments) from a holding potential of  $-60 \text{ mV}$ . Data were obtained before (control) and after the application of  $20 \mu\text{M}$  TTX. The inset shows the records of membrane current during the pulses to  $+20$ ,  $0$  and  $-20 \text{ mV}$  after the application of TTX at a slow time base. B, TTX-sensitive current. Top panel, superimposed records of TTX-sensitive currents obtained by subtraction of currents in the presence of TTX from those under control conditions. Bottom panel, current–voltage relationship of the peak inward TTX-sensitive current. All data from the same experiment.

Experiments to record  $i_{\text{Na}}$  were performed on a total of eighteen SA node cells from five rabbits ( $C_m$ , 21.8–61.5 pF; mean  $\pm$  s.e.m.,  $40.4 \pm 2.8$  pF,  $n = 18$ ). Sets of membrane currents recorded during depolarizing pulses from four of the cells are shown on the left of Fig. 9A. As shown in the top left-hand panel of Fig. 9A, in three out of the eighteen cells depolarizing pulses elicited only currents composed of transient outward current and  $i_{\text{Ca}}$ , and even when the holding potential was increased from  $-60$  to  $-80$  mV,  $i_{\text{Na}}$  was not activated. All the three cells were small in size with a capacitance ranging from 21.8 to 23.6 pF (Fig. 9B). In the

remaining fifteen cells ( $C_m > 28.5$  pF) depolarizing pulses activated  $i_{\text{Na}}$  (Fig. 9A).  $i_{\text{Na}}$  was completely abolished by  $20 \mu\text{M}$  TTX in all cells tested ( $n = 10$ ), and it was inhibited by  $81.6 \pm 1.3\%$  by  $2 \mu\text{M}$  TTX ( $n = 2$ ). Current–voltage relationships for the peak inward current ( $i_{\text{Na}}$ ) are shown on the right of Fig. 9A;  $i_{\text{Na}}$  density (current amplitude normalized by  $C_m$ ) is plotted against the membrane potential. The current–voltage relationships are similar in shape in the different cells, but the peak  $i_{\text{Na}}$  density at  $\sim -5$  mV increased with increase in cell size. The relationship between  $i_{\text{Na}}$  density at  $-5$  mV and cell capacitance in

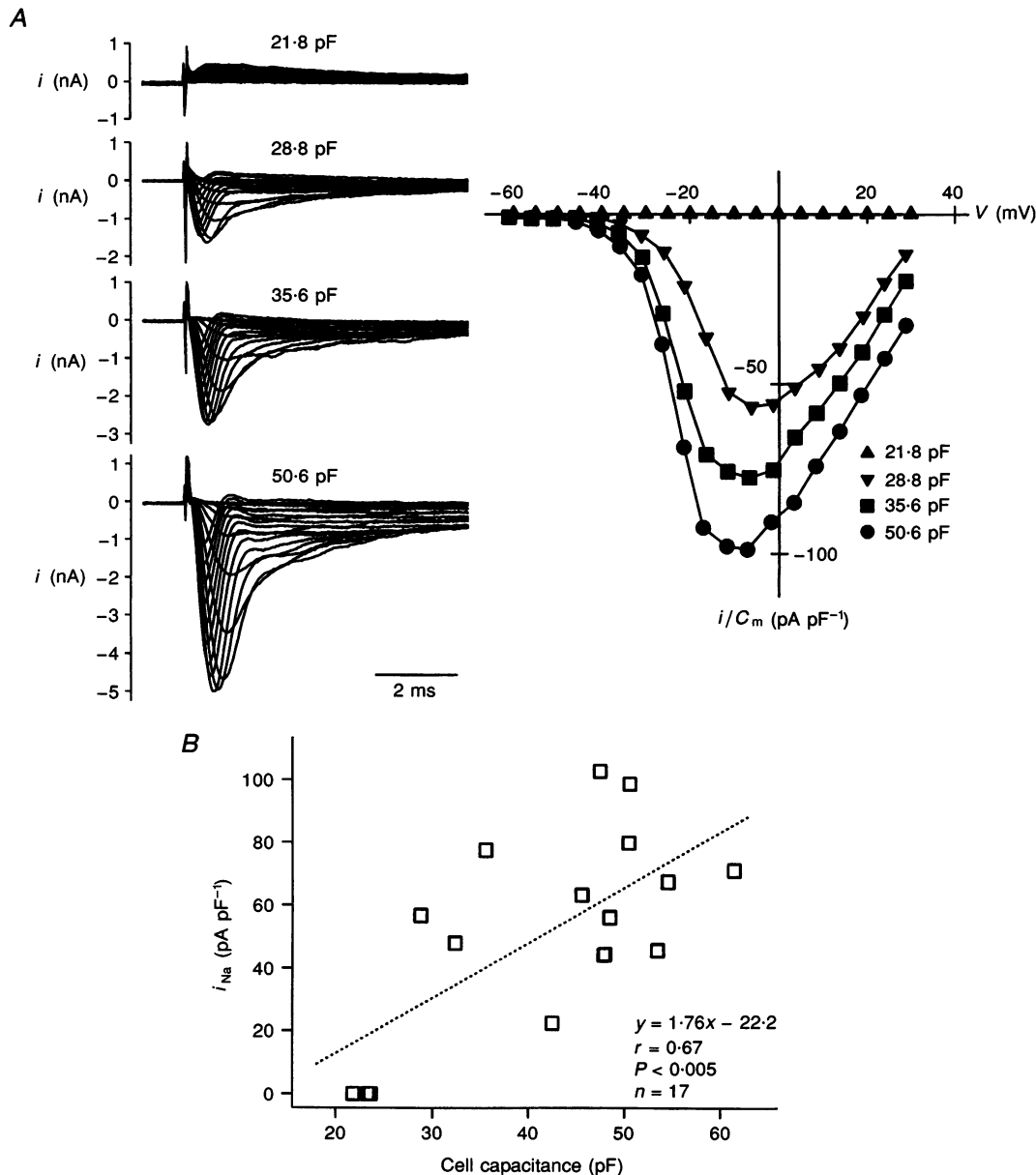


**Figure 9.** Correlation between the density of  $i_{\text{Na}}$  and cell size

**A**,  $i_{\text{Na}}$  in 4 SA node cells of different size. Left panel, superimposed records of membrane current in response to depolarizing voltage clamp pulses to various potentials (ranging from  $-55$  to  $+30$  mV in 5 mV increments) from the 4 cells. The cell capacitance is shown above each set of records. Right panel, current–voltage relationships for the peak inward current in the 4 cells. **B**, plot of the density of peak  $i_{\text{Na}}$  (current amplitude normalized by  $C_m$ ) measured at  $-5$  mV against cell capacitance in 17 SA node cells. The dotted line was fitted by linear regression.

seventeen SA node cells ( $C_m$ : mean  $\pm$  s.e.m.,  $41.1 \pm 2.8$  pF,  $n = 17$ ) is shown in Fig. 9B. The density of  $i_{Na}$  was significantly correlated with cell capacitance ( $r = 0.67$ ,  $P < 0.005$ ,  $n = 17$ );  $i_{Na}$  density was greater in larger SA node cells. In this statistical analysis, data obtained from one cell ( $C_m$ , 28.5 pF) out of a total of eighteen cells were excluded because the  $i_{Na}$  density in this cell ( $145.5$  pA pF $^{-1}$ ) was extraordinarily large and greater than the mean plus two standard deviations (mean  $\pm$  s.d. of  $i_{Na}$  density,  $56.9 \pm 36.8$  pA pF $^{-1}$ ,  $n = 18$ ).

## DISCUSSION

In the present study, the relationship between electrical activity and the size of cells isolated from the whole SA node region of the rabbit heart was investigated. All the data were obtained from spindle-shaped cells with regular and stable spontaneous activity. The characteristics of the cells (site of origin, cell shape and size, regular spontaneous beating, cell capacitance, presence of  $i_r$ , absence of  $i_{K,1}$ , high input resistance and action potential characteristics) prove that they are SA node pacemaker cells. We endeavoured to work only on single cells (rather than pairs or clusters). The fact that the distribution of cell capacitance could be reasonably well fitted by a normal distribution curve (Fig. 1) suggests that we were dealing with a population of single cells. Spider cells, similar to those described by DiFrancesco, Ferroni, Mazzanti & Tromba (1986) and Denyer & Brown (1990) were not included in the study because it is difficult to distinguish a genuine single cell from a pair or cluster of cells (Denyer & Brown, 1990). Some of the spider cells are genuine single cells (Verheijk, 1994) and we cannot exclude the possibility that we missed a population of cells with differing characteristics by not investigating spider cells.

The present study shows that various features of electrical activity are significantly correlated with cell capacitance, an index of cell size: in larger cells the MDP and the take-off potential were more negative, the action potential amplitude, the maximum upstroke velocity and the rate of diastolic depolarization were greater and the spontaneous cycle length was less. In all respects the electrical activity of the smaller cells matches that of small balls of tissue from the centre of the SA node and the electrical activity of the larger cells matches that of small balls of tissue from the periphery of the SA node (Kodama & Boyett, 1985). For example, in small balls of tissue from the centre of the rabbit SA node the maximum upstroke velocity was  $\sim 1.3$  V s $^{-1}$ , the action potential amplitude was  $\sim 47$  mV, the MDP was  $\sim -50$  mV and the spontaneous cycle length was  $\sim 352$  ms (compare with the data for small cells in Figs 3–5), whereas in small balls of tissue from the periphery the maximum upstroke velocity was  $\sim 41$  V s $^{-1}$ , the action potential amplitude was  $\sim 88$  mV, the MDP was  $\sim -71$  mV and the spontaneous cycle length was  $\sim 298$  ms (compare with the data for large cells in Figs 3–5) (Kodama & Boyett, 1985). Again, similar data to that from small and large cells have been obtained from

the intact SA node of the rabbit (Bleeker *et al.* 1980; Masson-Pévet *et al.* 1984). However, in this case the rate of diastolic depolarization decreases from the centre to the periphery (Bleeker *et al.* 1980; Masson-Pévet *et al.* 1984), whereas the rate of diastolic depolarization is greater in large cells (and also small balls of tissue from the periphery) than in small cells (or small balls from the centre) – this difference is considered below.

Previous morphological studies of the rabbit SA node tissue have shown that the size of pacemaker cells gradually increases from the leading pacemaker site in the centre of the SA node towards the periphery (Bleeker *et al.* 1980; Masson-Pévet *et al.* 1984; Opthof *et al.* 1987a; Oosthoek *et al.* 1993). Based on this, it is reasonable to hypothesize that the regional differences in electrical activity in the intact SA node (and in the small balls of tissue) are the result of a cell size-dependent variation in electrical activity. This is contrary to the hypothesis of Verheijk (1994), in which he suggested that the electrical activity of SA node cells is uniform and regional differences in the intact SA node are the result of a variable mix between SA node and atrial cells. Although we have shown that SA node cells are heterogeneous, we cannot rule out the possibility that the mixing of atrial with SA node cells may influence the properties of the SA node.

Doerr, Denger & Trautwein (1989) isolated two functionally different types of pacemaker cells from the rabbit SA node; one from the centre showed a slower upstroke, a smaller action potential and a less negative MDP than the other from the periphery of the SA node. However, these investigators did not mention the morphology of the two types of SA node cells. In cell culture Nathan (1986) also identified two morphologically distinct spontaneously beating cell types from the rabbit SA node (types I and II). Type I cells were spindle shaped and weakly beating, and the action potential had a low maximum upstroke velocity ( $\sim 3$  V s $^{-1}$ ). Type II cells were perhaps originally rod shaped (although they rounded up in cell culture) and strongly beating, and the action potential had a high upstroke velocity ( $\sim 32$  V s $^{-1}$ ). Both the results of Doerr *et al.* (1989) and Nathan (1986) are consistent with the results of the present study.

Our working hypothesis is that the smaller cells may dominate the centre of the SA node, whereas larger cells may dominate the periphery. The present results, however, show that the spontaneous cycle length was shorter for large cells. In experiments on small balls of tissue from the rabbit SA node, in which this electrotonic interaction is removed, Kodama & Boyett (1985) also showed spontaneous activity of balls from the periphery was faster than that of balls from the centre. Similar results were reported by Opthof *et al.* (1987b) in experiments using small tissue preparations dissected from the rabbit SA node. This apparent paradox can be explained by electrotonic interaction between pacemaking SA node cells in the periphery and the surrounding non-pacemaking atrial cells in the intact SA

node. Recently, we demonstrated in isolated rabbit SA node cells that the spontaneous activity of an SA node cell is easily inhibited when the cell is coupled to a membrane model of an atrial cell (Watanabe *et al.* 1995). Further support for electrotonic inhibition of the periphery of the SA node by the surrounding atrial muscle has also been provided by other studies (Kirchhof, Bonke, Allesie & Lammers, 1987; Winslow, Kimball, Varghese & Noble, 1993).

We measured  $i_f$ ,  $i_{Ca}$  and  $i_{Na}$  in a wide range of different sized SA node cells ( $C_m$ , 21.8–61.5 pF). The results have revealed that the larger the cell capacitance the greater the density of  $i_f$  and  $i_{Na}$ , although there was no such cell size-dependent variation in the density of  $i_{Ca}$ . To the best of our knowledge, this is the first report demonstrating a relationship between morphology and ionic currents in isolated pacemaker cells from the mammalian SA node. A new sustained inward current ( $i_{st}$ ) has been demonstrated in single rabbit SA node cells by Guo, Ono & Noma (1995) and the authors commented that the current was only recorded in typical SA node cells ( $C_m$ ,  $47 \pm 14$  pF) and not in 'transitional' ('peripheral' in the terminology of the present study) SA node cells.

The greater rate of diastolic depolarization and the faster spontaneous activity (shorter spontaneous cycle length) of larger cells may be attributed at least in part to the greater density of  $i_f$  in larger cells. Nikmaram, Boyett, Kodama & Suzuki (1995) investigated the effects of different  $i_f$  blockers (2 mM Cs<sup>+</sup>, 1  $\mu$ M UL-FS 49 and 3  $\mu$ M ZD 7288) on the pacemaker potential in different regions of the intact SA node of the rabbit. The reduction of the rate of diastolic depolarization was minimal in the centre (~22 to ~25%) and maximal (~69 to ~120%) in the periphery. They also examined the effects of 2 mM Cs<sup>+</sup> on small balls of tissue from different regions of the SA node. The Cs<sup>+</sup>-induced reduction in the rate of diastolic depolarization and the increase in spontaneous cycle length were greatest in balls from the periphery and least in balls from the centre. Similar regional differences of Cs<sup>+</sup> action in small multicellular tissue preparations of rabbit SA node were also reported by Kreitner (1985). The data of Nikmaram *et al.* (1995) and Kreitner (1985) are consistent with the results from the present study.

In the present study, the take-off potential was relatively positive (~–45 mV) and the maximum upstroke velocity was low (less than 10 V s<sup>-1</sup>) in small SA node cells with a capacitance of less than ~25 pF, whereas in larger cells the take-off potential was more negative (~–55 mV) and the maximum upstroke velocity could be dramatically greater (more than 60 V s<sup>-1</sup>). The relatively positive take-off potential and low maximum upstroke velocity in small cells can be explained by the absence of  $i_{Na}$  in these cells; in these cells  $i_{Ca}$  is presumably responsible for the upstroke.  $i_{Ca}$  has a threshold of ~–40 mV and is relatively small in amplitude (in comparison with  $i_{Na}$ ) and thus the relatively positive take-off potential and low upstroke velocity can be

explained. The relatively negative take-off potential and high upstroke velocity of larger cells can be explained by the presence of  $i_{Na}$  (the threshold of  $i_{Na}$  is ~–60 mV, thus explaining the more negative take-off potential, and  $i_{Na}$  is larger than  $i_{Ca}$ , thus explaining the higher maximum upstroke velocity). In larger cells, not only is the  $i_{Na}$  density greater, but the more negative diastolic potentials will mean that there will be less inactivation of  $i_{Na}$ .

Baruscotti, DiFrancesco & Robinson (1996) recently investigated age-dependent changes in  $i_{Na}$  in rabbit SA node cells. In their experiments,  $i_{Na}$  was present in SA node cells isolated from newborn rabbits, whereas  $i_{Na}$  was absent in SA node cells obtained from adult rabbits. The apparent discrepancy between their data showing the absence of  $i_{Na}$  in adult SA node cells and ours indicating the presence of  $i_{Na}$  in adult rabbit SA node cells can be explained by the cell size-dependent differences in  $i_{Na}$ . Baruscotti *et al.* (1996) used small SA node cells with a capacitance of ~20 pF. In the present study  $i_{Na}$  was also absent in cells with this capacitance.  $i_{Na}$  present in rabbit SA node cells has also been reported by Denyer & Brown (1990) and Oei, van Ginneken, Jongasma & Bouman (1989). In the study of Nathan (1986) on cultured rabbit SA node cells, the type II cells (possibly peripheral – see above), but not the type I cells (possibly central), possessed  $i_{Na}$ . In experiments on multicellular preparations of the SA node, the maximum upstroke velocity was markedly reduced by TTX in the periphery, but not the centre, of the SA node (Kreitner, 1985; Lipsius & Vassalle, 1987). In a recent study of small balls of rabbit SA node tissue, TTX caused a decrease in the maximum upstroke velocity to less than 10% in peripheral tissue, whereas it had no significant effect on the upstroke in central tissue (Nikmaram, Kodama, Boyett, Suzuki & Honjo, 1996). In small balls of tissue taken from the periphery (but not from the centre) of the SA node, TTX also shifted the take-off potential from ~–60 to ~–45 mV and as a result of this the spontaneous cycle length was prolonged by ~150%. Such regional differences in the action of TTX can be explained by the cell size-dependent differences in  $i_{Na}$  density demonstrated in the present study. It is concluded from this that the increase in the density of  $i_{Na}$  in large cells is possibly not only responsible for the more negative take-off potential and higher maximum upstroke velocity in the periphery of the SA node, but also partly responsible for the faster intrinsic pacemaker activity in the periphery.

Although this study has highlighted cell size-dependent variation in the density of  $i_f$  and  $i_{Na}$  in the region-dependent changes in electrical activity within the SA node, we cannot rule out possible differences in other ionic currents that are involved in pacemaker activity in SA node cells, such as delayed rectifier K<sup>+</sup> current (Ito & Ono, 1995; Ono & Ito, 1995; Verheijck, van Ginneken, Bourier & Bouman, 1995), T-type Ca<sup>2+</sup> current ( $i_{Ca,T}$ ; Hagiwara, Irisawa & Kameyama, 1988; Doerr *et al.* 1989) and background currents (Hagiwara, Irisawa, Kasanuki & Hosoda,

1992; Ito, Ono & Noma, 1994; Guo, Ono & Noma, 1995; Sakai, Hagiwara, Matsuda, Kasanuki & Hosoda, 1996). For example, Hagiwara *et al.* (1988) have shown that the density of  $i_{Ca,T}$  in rabbit SA node cells is much larger (approximately 10 times larger) than that in atrial cells, and Doerr *et al.* (1989) have reported a marked cell-to-cell variation in the negative chronotropic effect of selective  $i_{Ca,T}$  blockade (by  $40 \mu\text{M}$   $\text{Ni}^{2+}$ ). These findings suggest differences in the density of  $i_{Ca,T}$  in SA node cells.

Although the centre of the SA node is the leading pacemaker site under normal conditions, it is well known that the leading pacemaker site shifts to a more peripheral part of the SA node in various circumstances (fall in temperature, fall in extracellular  $\text{Ca}^{2+}$ , application of cardiac glycoside, adrenaline or ACh, parasympathetic and sympathetic stimulation, block of  $i_{Ca}$  or the rapid delayed rectifier  $\text{K}^+$  current,  $i_{K,r}$  – Bouman, Mackaay, Bleeker & Becker, 1978; Steinbeck, Bonke, Alessie & Lammers, 1978; Mackaay, Opthof, Bleeker, Jongasma & Bouman, 1980; Verheijck, 1994). ‘Pacemaker shift’ presumably occurs because the pacemaker activity of different regions of the SA node is differentially affected by interventions, and this in turn must be a consequence of the regional differences in ionic mechanisms underlying pacemaker activity that we have begun to explore in the present study. The data of Baruscotti *et al.* (1996) suggest that the  $\text{Na}^+$  channel is distributed throughout the SA node of the newborn rabbit, whereas the data from the present study suggests that in the adult rabbit (~2–3 months old) the  $\text{Na}^+$  channel may be absent in the centre and only present in the periphery of the SA node (as a result the upstroke velocity is low in the centre and high in the periphery as discussed above). Alings & Bouman (1993) reported that in the rabbit the area of the SA node with an upstroke velocity of less than  $5 \text{ V s}^{-1}$  increases 27 times with age (up to 5 years). This is presumably the result of a further reduction in the expression of the  $\text{Na}^+$  channel in the SA node. Alings & Bouman (1993) suggested that this may help to explain the well known age-related dysfunction of the SA node. This raises the possibility that upregulation of the  $\text{Na}^+$  channel in the SA node may help to rectify age-related dysfunction of the SA node.

In conclusion, in the present study we have demonstrated that the rabbit SA node is composed of electrophysiologically heterogeneous pacemaker cells with different electrical membrane properties; the densities of  $i_f$  and  $i_{\text{Na}}$  are higher in larger SA node cells than in smaller cells, whereas the density of  $i_{Ca}$  is cell size independent. The similar voltage dependence of activation of  $i_f$  and  $i_{\text{Na}}$  in cells of different size suggests that the greater current density is probably the result of a higher expression of functional channels on the cytoplasmic membrane. The cell size-dependent differences in ionic currents may underlie regional differences in electrical activity within the SA node. However, the differences in  $i_f$  and  $i_{\text{Na}}$  densities cannot explain some of the regional differences in electrical activity within the SA node

(such as the variation in the MDP), and differences in other ionic currents may also contribute to the regional differences in electrical activity. To elucidate these differences, further studies will be required.

- ALINGS, A. M. W. & BOUMAN, L. N. (1993). Electrophysiology of the ageing rabbit and cat sinoatrial node – a comparative study. *European Heart Journal* **14**, 1278–1288.
- BARUSCOTTI, M., DI FRANCESCO, D. & ROBINSON, R. B. (1996). A TTX-sensitive inward sodium current contributes to spontaneous activity in newborn rabbit sino-atrial node cells. *Journal of Physiology* **492**, 21–30.
- BLEEKER, W. K., MACKAAY, A. J. C., MASSON-PÉVET, M., BOUMAN, L. N. & BECKER, A. E. (1980). Functional and morphological organization of the rabbit sinus node. *Circulation Research* **46**, 11–22.
- BOUMAN, L. N., MACKAAY, A. J. C., BLEEKER, W. K. & BECKER, A. E. (1978). Pacemaker shift in the sinus node: effects of vagal stimulation, temperature and reduction of extracellular calcium. In *The Sinus Node, Structure, Function and Clinical Relevance*, ed. BONKE, F. I. M., pp. 245–257. Martinus Nijhoff, The Hague, Boston, London.
- DENYER, J. C. (1989). Isolation and electrophysiological characteristics of rabbit sino-atrial node cells. PhD Thesis, University of Oxford.
- DENYER, J. C. & BROWN, H. F. (1990). Rabbit sino-atrial node cells: isolation and electrophysiological properties. *Journal of Physiology* **428**, 405–424.
- DI FRANCESCO, D., FERRONI, A., MAZZANTI, M. & TROMBA, C. (1986). Properties of the hyperpolarizing-activated current ( $i_f$ ) in cells isolated from the rabbit sino-atrial node. *Journal of Physiology* **377**, 61–88.
- DOERR, T., DINGER, R. & TRAUTWEIN, W. (1989). Calcium currents in single SA nodal cells of the rabbit heart studied with action potential clamp. *Pflügers Archiv* **413**, 599–603.
- GILES, W. R. & VAN GINNEKEN, A. C. G. (1985). A transient outward current in isolated cells from the crista terminalis. *Journal of Physiology* **368**, 243–264.
- GUO, J., ONO, K. & NOMA, A. (1995). A sustained inward current activated at the diastolic potential range in rabbit sino-atrial node cells. *Journal of Physiology* **483**, 1–13.
- HAGIWARA, N., IRISAWA, H. & KAMEYAMA, M. (1988). Contribution of two types of calcium currents to the pacemaker potentials of rabbit sino-atrial node cells. *Journal of Physiology* **395**, 233–253.
- HAGIWARA, N., IRISAWA, H., KASANUKI, H. & HOSODA, S. (1992). Background current in sino-atrial node cells of the rabbit heart. *Journal of Physiology* **448**, 53–72.
- HONJO, H. & BOYETT, M. R. (1992). Correlation between action potential parameters and the size of single sino-atrial node cells isolated from the rabbit heart. *Journal of Physiology* **452**, 128P.
- HONJO, H., BOYETT, M. R. & KODAMA, I. (1996). The density of the TTX-sensitive  $\text{Na}^+$  current and the hyperpolarization-activated current in rabbit sinoatrial node cells depends on cell size. *Journal of Physiology* **491.P**, 154P.
- HONJO, H., KODAMA, I., ZANG, W.-J. & BOYETT, M. R. (1992). Desensitization to acetylcholine in single sinoatrial node cells isolated from rabbit hearts. *American Journal of Physiology* **263**, H1779–1789.
- IRISAWA, H., BROWN, H. F. & GILES, W. (1993). Cardiac pacemaking in the sinoatrial node. *Physiological Reviews* **73**, 197–227.

- ITO, H. & ONO, K. (1995). A rapidly activating delayed rectifier K<sup>+</sup> channel in rabbit sinoatrial node cells. *American Journal of Physiology* **269**, H443–452.
- ITO, H., ONO, K. & NOMA, A. (1994). Background conductance attributable to spontaneous opening of muscarinic K<sup>+</sup> channels in rabbit sino-atrial node cells. *Journal of Physiology* **476**, 55–68.
- JAMES, T. N. (1967). Anatomy of the cardiac conduction system in the rabbit. *Circulation Research* **20**, 638–648.
- KIRCHHOF, C. J. H. J., BONKE, F. I. M., ALLESSIE, M. A. & LAMMERS, W. J. E. P. (1987). The influence of the atrial myocardium on impulse formation in the rabbit sinus node. *Pflügers Archiv* **410**, 198–203.
- KODAMA, I. & BOYETT, M. R. (1985). Regional differences in the electrical activity of the rabbit sinus node. *Pflügers Archiv* **404**, 214–226.
- KREITNER, D. (1985). Electrophysiological study of the two main pacemaker mechanisms in the rabbit sinus node. *Cardiovascular Research* **19**, 304–318.
- LIPSIVS, S. L. & VASSALLE, M. (1978). Characterization of a two-component upstroke in the sinus node subsidiary pacemakers. In *The Sinus Node: Structure, Function and Clinical Relevance*, ed. BONKE, F. I. M., pp. 233–244. Martinus Nijhoff, The Hague, Boston, London.
- MACKAAY, A. J. C., OPTHOF, T., BLEEKER, W. K., JONGSMA, H. J. & BOUMAN, L. N. (1980). Interaction of adrenaline and acetylcholine on cardiac pacemaker function: functional inhomogeneity of the rabbit sinus node. *Journal of Pharmacology and Experimental Therapeutics* **214**, 417–422.
- MASSON-PÉVET, M. A., BLEEKER, W. K., BESSELSSEN, E., TREYTEL, B. W., JONGSMA, H. J. & BOUMAN, L. N. (1984). Pacemaker cell types in the rabbit sinus node: a correlative ultrastructural and electrophysiological study. *Journal of Molecular and Cellular Cardiology* **16**, 53–63.
- MASSON-PÉVET, M., BLEEKER, W. K., MACKAAY, A. J. C., BOUMAN, L. N. & HOUTKOOPEER, J. M. (1979). Sinus node and atrium cells from the rabbit heart: a quantitative electron microscopic description after electrophysiological localization. *Journal of Molecular and Cellular Cardiology* **11**, 555–568.
- NATHAN, R. D. (1986). Two electrophysiologically distinct types of cultured pacemaker cells from rabbit sinoatrial node. *American Journal of Physiology* **250**, H325–329.
- NIKMARAM, M. R., BOYETT, M. R., KODAMA, I. & SUZUKI, R. (1995). Regional differences in the role of the hyperpolarization-activated current, *i<sub>h</sub>*, in the pacemaker potential in the isolated sinoatrial node of the rabbit. *Journal of Physiology* **487**, P. 126–127P.
- NIKMARAM, M. R., KODAMA, I., BOYETT, M. R., SUZUKI, R. & HONJO, H. (1996). The Na<sup>+</sup> current plays an important role in pacemaker activity in the periphery, but not the centre, of the rabbit sinoatrial node. *Journal of Physiology* **491**, P. 154P.
- OEI, H. I., VAN GINNEKEN, A. C. G., JONGSMA, H. J. & BOUMAN, L. N. (1989). Mechanisms of impulse generation in isolated cells from the rabbit sinoatrial node. *Journal of Molecular and Cellular Cardiology* **21**, 1137–1149.
- ONO, K. & ITO, H. (1995). Role of rapidly activating delayed rectifier K<sup>+</sup> current in sinoatrial node pacemaker activity. *American Journal of Physiology* **269**, H453–462.
- OOSTHOEK, P. W., VIRÁGH, S., MAYEN, A. E. M., VAN KEMPEN, M. J. A., LAMERS, W. H. & MOORMAN, A. F. M. (1993). Immunohistochemical delineation of the conduction system I: the sinoatrial node. *Circulation Research* **73**, 473–481.
- OPTHOF, T., DE JONGE, B., MACKAAY, A. J. C., BLEEKER, W. K., MASSON-PÉVET, M., JONGSMA, H. J. & BOUMAN, L. N. (1985). Functional and morphological organization of the guinea-pig sinoatrial node compared with the rabbit sinoatrial node. *Journal of Molecular and Cellular Cardiology* **17**, 549–564.
- OPTHOF, T., DE JONGE, B., MASSON-PÉVET, M., JONGSMA, H. J. & BOUMAN, L. N. (1986). Functional and morphological organization of the cat sinoatrial node. *Journal of Molecular and Cellular Cardiology* **18**, 1015–1031.
- OPTHOF, T., DE JONGE, B., JONGSMA, H. J. & BOUMAN, L. N. (1987a). Functional morphology of the pig sinoatrial node. *Journal of Molecular and Cellular Cardiology* **19**, 1221–1236.
- OPTHOF, T., VAN GINNEKEN, A. C. G., BOUMAN, L. N. & JONGSMA, H. J. (1987b). The intrinsic cycle length in small pieces isolated from the rabbit sinoatrial node. *Journal of Molecular and Cellular Cardiology* **19**, 923–934.
- SAKAI, R., HAGIWARA, N., MATSUDA, N., KASANUKI, H. & HOSODA, S. (1996). Sodium-potassium pump current in rabbit sino-atrial node cells. *Journal of Physiology* **490**, 51–62.
- STEINBECK, G., BONKE, F. I. M., ALLESSIE, M. A. & LAMMERS, W. J. E. P. (1978). Cardiac glycosides and pacemaker activity of the sinus node – a microelectrode study on the isolated right atrium of the rabbit. In *The Sinus Node, Structure, Function and Clinical Relevance*, ed. BONKE, F. I. M., pp. 258–269. Martinus Nijhoff, The Hague, Boston, London.
- TRANUM-JENSEN, J. (1976). The fine structure of the atrial and atrioventricular (AV) junctional specialized tissues of the rabbit heart. In *The Conduction System of the Heart*, ed. WELLENS, H. J. J., LIE, K. I. & JANSE, M. J., pp. 55–81. Stenfert Kroese BV, Leiden.
- TEN VELDE, I., DE JONGE, B., VERHEIJCK, E. E., VAN KEMPEN, M. J. A., ANALBERS, L., GROS, D. & JONGSMA, H. J. (1995). Spatial distribution of connexin 43, the major cardiac gap junction protein, visualizes the cellular network for impulse propagation from sinoatrial node to atrium. *Circulation Research* **76**, 802–811.
- VERHEIJCK, E. E. (1994). Pacemaker currents in the sino-atrial node. PhD Thesis, University of Amsterdam.
- VERHEIJCK, E. E., VAN GINNEKEN, A. C. G., BOURIER, J. & BOUMAN, L. N. (1995). Effects of delayed rectifier current blockade by E-4031 on impulse generation in single sinoatrial nodal myocytes of the rabbit. *Circulation Research* **76**, 607–615.
- WATANABE, E., HONJO, H., ANNO, T., BOYETT, M. R., KODAMA, I. & TOYAMA, J. (1995). Modulation of pacemaker activity of sinoatrial node cells by electrical load imposed by an atrial cell model. *American Journal of Physiology* **269**, H1735–1742.
- WINSLOW, R. L., KIMBALL, A. L., VARGHESE, A. & NOBLE, D. (1993). Simulating cardiac sinus and atrial network dynamics on the connection machine. *Physica D* **64**, 281–298.

#### Acknowledgements

This work was supported by the British Heart Foundation, The Wellcome Trust, the British Council and the International Scientific Research Program of the Ministry of Education, Science and Culture of Japan.

#### Authors' email addresses

M. R. Boyett: m.r.boyett@leeds.ac.uk

H. Honjo: honjo@riem.nagoya-u.ac.jp

Received 16 April 1996; accepted 27 July 1996.